C. R. Mecanique 342 (2014) 714–725

Contents lists available at ScienceDirect

Comptes Rendus Mecanique

www.sciencedirect.com

Three-dimensional Rayleigh–Bénard magnetoconvection: Effect of the direction of the magnetic field on heat transfer and flow patterns

Awatef Naffouti *, Brahim Ben-Beya, Taieb Lili

Laboratoire de mécanique des fluides, Faculté des sciences de Tunis, Département de physique, 2092 El Manar 2, Tunis, Tunisia

ARTICLE INFO

Article history:
Received 26 May 2014
Accepted 4 September 2014
Available online 20 September 2014

Keywords:
Heat transfer
Magnetoconvection
Rayleigh–Bénard
Cubical cavity

ABSTRACT

The effect of an imposed magnetic field on Rayleigh–Bénard three-dimensional natural convection was investigated numerically. The cubical cavity is heated from below and cooled from above, and the remaining side walls are insulated. The magnetic field is tilted at an angle α about the horizontal. Flow field and heat transfer were predicted for fluid with $Pr = 0.71$ and a wide range of governing parameters such as a Rayleigh number between 5×10^4 and 10^5, a Hartmann number between 0 and 60, and an inclination angle between 0° and 360°. When a magnetic field is applied on a non-conducting fluid within a cubical cavity, whether the natural convection is promoted or damped is found to depend on both the direction and the magnitude of the magnetic field. The average Nusselt number decreased with an increase of the Hartmann number and increased with an increase of the Rayleigh number. The maximum heat transfer rate was observed for $\alpha = 30°$ and $Ha = 10$, while heat transfer was poor for the vertical direction of the magnetic field. The dependence of the promotion or damping efficiency on α and Ha is also discussed in terms of isocontours and isosurfaces in sight of the dynamic and thermal behaviour of the flow.

1. Introduction

Buoyancy-driven flows heated from below, known as Rayleigh–Bénard (RB) phenomena, have always received considerable attention due to their wide variety of applications in engineering and technology [1–3]. RB convection is an extensively studied system for investigating instabilities, bifurcation, spatiotemporal chaos, and turbulence [4].

In many scientific and industrial applications, it is often necessary to control convective flows induced by natural convection in order to achieve specific outcomes. Such control can be achieved using an imposed external magnetic field, and this falls under what is called magnetoconvection.

Magnetoconvection in enclosures particularly has applications in solar technologies, crystal growth in liquids, material manufacturing technology, nuclear reactor insulation, haemodialysis, etc. It also occurs under many circumstances and plays an important role in geophysics, astrophysics, aerodynamics, engineering, and industries [5–7]. Most of the early works on magnetoconvection are summarized in a book by Ozoe [8]. Flow modes as well as heat transfer characteristics associated

* Corresponding author.
E-mail address: awatef.naffouti@yahoo.fr (A. Naffouti).

http://dx.doi.org/10.1016/j.crme.2014.09.001
1631-0721/

Nomenclature

a	thermal diffusivity (m^2/s)
B	dimensional magnetic induction (Tesla)
E	electrical field ($V \cdot m^{-1}$)
g	acceleration of gravity ($m \cdot s^{-2}$)
H	height of the enclosure (m)
L	length of the enclosure (m)
Ha	Hartmann number ($Ha = BL(\sigma/\mu)^{1/2}$)
J	electric current
$\overline{Nu}$	average Nusselt number, defined in Eq. (12)
p	pressure (N/m^2)
P	dimensionless pressure, $P = pL^2/\rho a^2$
Pr	Prandtl number, $Pr = \nu/a$
Gr	Grashof number, $Gr = \frac{Ra}{Pr}$
Ra	Rayleigh number, $Ra = gL^3\beta_T(T_H - T_C)/(\nu a)$
Ra_C	critical Rayleigh number
T_C	cold wall temperature (K)
T_H	hot wall temperature (K)
T	temperature (K)
τ	dimensional time (s)
U, V, W	velocity components in x, y, z directions ($m \cdot s^{-1}$)
u, v, w	dimensionless velocity components in x, y, z directions
x, y, z	dimensionless Cartesian coordinates

Greek symbols

β	coefficient of thermal expansion (K^{-1})
Δ	difference value
θ	dimensionless temperature, $\theta = (T - T_0)/(T_H - T_C)$
ν	kinematics viscosity ($m^2 \cdot s^{-1}$)
μ	dynamic viscosity ($kg \cdot m^{-1} \cdot s^{-1}$)
ρ	fluid density ($kg \cdot m^{-3}$)
t	dimensionless time, $t = \tau a/L^2$
Φ	dimensionless variable (u, v, p, θ)
σ	electrical conductivity ($\Omega^{-1} \cdot m$)

Subscripts

max	maximum
0	reference value
C	cold
H	hot

with Rayleigh–Bénard magnetoconvection (RBM) have been a subject of interest to engineers and scientists for many years [9–11].

Magnetoconvection in enclosures has continued to be a very active area for scientists during the past few decades. For example, Alchaar et al. [12] studied numerically the RBM flow within a shallow cavity filled with an electrically conducting fluid under a uniform magnetic field. The investigation covers the range of the Rayleigh number, Ra, from 1.8×10^3 to 3×10^4, of the Hartmann number, Ha, from 0 to 35, with an aspect ratio of the cavity of 6. The authors showed that the magnetic field reduces the convective heat transfer through the cavity. Furthermore, the numerical results indicate that the magnetic field, as expected, inhibits the onset of convection. Sophy et al. [13] analysed the magnetoconvection flow in a differentially heated square cavity for Rayleigh numbers ranging from 10^3 to 10^5. They demonstrated that a great modification of the flow pattern occurs when the maximum value of the magnetic field is beyond a critical one. Ece and Büyük [14] examined the effects of the applied magnetic field in an inclined rectangular enclosure heated from the left vertical wall and cooled from the top wall, on the heat transfer rate and the flow patterns. They argued that the flow characteristics and therefore the convection heat transfer depend strongly upon the strength and direction of the magnetic field, the aspect ratio and the inclination of the enclosure. Therefore, the magnetic field significantly reduces the heat transfer rate by suppressing the convection currents.

The effects of a magnetic field on the buoyancy-driven convection in differentially heated square enclosure have been studied by Pirmohammadi et al. [9]. They approved that the heat transfer mechanisms and the flow patterns within the enclosure depend strongly upon both the strength of the magnetic field as well as the Rayleigh number. It was concluded that the magnetic field considerably decreases the average Nusselt number. In another work, the same authors, conducted a steady, laminar, RBM in a tilted enclosure filled with liquid gallium [15]. It is shown that for a given inclination angle of the cavity, as the value of the Hartmann number increases, the heat transfer rate diminishes. Furthermore, it is found that at high Ra values, the average Nusselt number depends strongly on the inclination angle for relatively small values of the Hartmann number. From a numerical study viewpoint, the works of Lo [16] disclosed that, for a constant value of the Grashof number within a differentially heated cavity with a transverse magnetic field, the heat transfer rate is at its maximum for higher Pr values and in the absence of magnetic field ($Ha = 0$), while it is lower with increasing the strength of the external magnetic field in the lower region of the Prandtl number.

In the above-mentioned studies, two-dimensional models were used to simulate a magnetoconvection flow inside enclosures. However, depending on the dimensions of the cavity, significant three-dimensional effects can arise. The literature was relatively scarce in what concerns research work dealing with magnetoconvection in three-dimensional configurations. Nowadays, with the advent of computer technology, numerical studies of heat transfers and fluid flows within 3D enclosures are becoming feasible and more common. For instance, three-dimensional magnetoconvection in a cubic enclosure heated from one wall and cooled from an opposing one have been performed by Ozoe and Okada as soon as 1989 [17]. Their results showed that horizontal magnetic fields are the most effective in suppressing convection. In contrast, vertical magnetic fields are found to be least effective.

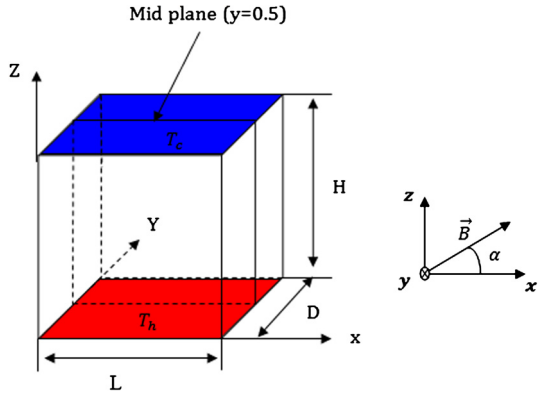

Fig. 1. (Colour online.) Three-dimensional Rayleigh–Bénard configuration.

Mobner and Muller [18] studied the influence of uniform magnetic fields of arbitrary direction on three-dimensional natural convection in liquid metals. The convection can be driven by horizontal or vertical temperature gradients. For a vertical temperature gradient, the authors demonstrated the fact that the number of convection rolls depends on both the Rayleigh and the Hartmann parameters. Increasing the Rayleigh and Hartmann numbers' values augments the number of convection rolls in the enclosure. Piazza and Ciofalo [19] discussed 3D magnetoconvection in a liquid-metal-filled cubic enclosure for which a uniform magnetic field was applied orthogonally to the gravity vector. The effects of the Hartmann number and of the wall conductance ratio were investigated. In particular, they concluded that increasing *Ha* suppressed convective motions and exalted the square shape of the circulation cells. Kenjereš and Hanjalić [20] reported a numerical study of the effects of magnitude and distribution of an external magnetic field on the reorganization of convective structures and heat transfer in thermal convection in electrically conductive fluids. The results reveal, in the case of RB convection, that a vertical homogeneous magnetic field causes a strong reduction in both the integral and the local heat transfer coefficients, while in a spanwise field the effect is weaker. Xu et al. [21] experimentally showed that natural convection in a three-dimensional enclosure filled with gallium and differentially heated is suppressed with an imposed magnetic field, and the damping effect increases as the magnetic field's strength increases. The convection of a paramagnetic fluid under a strong magnetic field in a cubical enclosure heated and cooled from two opposite walls has been investigated experimentally and numerically by Bednarz et al. [22]. A transverse horizontal magnetic field is applied to the system. The authors argued that by using a strong magnetic field, convection could be suppressed or inverted with different combinations of the two main body forces. The effect of a magnetic field on the onset of time-periodic convection was addressed numerically by Henry et al. [23] in a three-dimensional enclosure. The authors demonstrated the large dependencies of both the critical Grashof number and the frequency at the Hopf bifurcation point on the imposed magnetic field. Recently, Varshney and Baig [24] investigated the effect of constant transverse magnetic field on rotating Rayleigh–Bénard convection of an electrically conducting fluid ($Pr = 0.01$). Among several results, the authors demonstrated the production of anisotropy if a transverse magnetic field was applied to the cavity.

Among the studies mentioned above, several works refer to the magnetoconvection flow inside enclosures for which the direction of the applied magnetic field is usually kept parallel or orthogonal to the thermal gradient. However, some works revealed that magnetic field direction has effects on the flow and heat transfer rates in a cavity. For example, Sivasankaran and Ho [25] studied the natural convection of maximum density water in the presence of a magnetic field with temperature-dependent properties in a cavity and argued that the external magnetic field direction is an important parameter for fluid flow as well as for heat transfer. Recently, Bouabdallah and Bessaih [26] carried out an investigation to analyse the effect of a magnetic field on a three-dimensional fluid flow and heat transfer during solidification from a melt in a cubic enclosure. The results exhibited a strong relationship between the interface shape, the magnitude and orientation of the magnetic field.

To the author's knowledge, studies have thus far addressed three-dimensional RBM under an applied magnetic field for which the direction is changed. The objective of the present paper is therefore to predict the effect of the direction of the magnetic field on three-dimensional Rayleigh–Bénard convection. In particular, the effects of the magnetic field parameter (Ha) and of the Rayleigh number (Ra) on the relevant flow variables are described in detail.

2. Physical model and mathematical formulation

Fig. 1 displays schematically the configuration of the three-dimensional enclosure considered in this study. The enclosure with length L is heated from below at T_H and cooled from above at T_C; the remaining vertical walls are assumed thermally adiabatic. It is further assumed that the Boussinesq approximation is valid for the buoyancy force. The cubic enclosure is filled with a viscous, incompressible and electrically conducting fluid which is permeated by a uniform magnetic field **B** with magnitude proportional to *Ha* at an inclined angle α from the horizontal plane.

$$\nabla \cdot V = 0 \tag{1}$$

$$\frac{\partial V}{\partial \tau} + (V \cdot \nabla)V = -\frac{1}{\rho}\nabla p + \nu \nabla^2 V - \beta(T - T_C)g + \frac{1}{\rho} J \times B \tag{2}$$

$$\frac{\partial T}{\partial \tau} + (V \cdot \nabla T) = a\nabla^2 T \tag{3}$$

where the electric current J is given by:

$$J = \sigma(E + V \times B) \tag{4}$$

Here $V(u, v, w)$ is the fluid velocity vector, $\mathbf{B}(B_x, 0, B_z)$ is the external magnetic field, $\mathbf{E}$ is the electric field, p is pressure, and T is the fluid's temperature. ∇ is the gradient operator and ρ denotes the density of the fluid, whereas ν, a, and β are the cinematic viscosity, the thermal diffusivity coefficient, and the thermal expansion coefficient, respectively. The electric conductivity of the electric fluid is noted by σ. As the electric field vanishes everywhere in the cavity, the effect of E is neglected. In addition, the magnetic Reynolds number is assumed to be small so that the induced magnetic field can be neglected. Under the above assumption, the usual three-dimensional governing equations for the unsteady magnetoconvection flow, in dimensionless form, can be written as:

$$\frac{\partial u}{\partial x} + \frac{\partial v}{\partial y} + \frac{\partial w}{\partial z} = 0 \tag{5}$$

$$\frac{\partial u}{\partial t} + u\frac{\partial u}{\partial x} + v\frac{\partial u}{\partial y} + w\frac{\partial u}{\partial z} = -\frac{\partial p}{\partial x} + Pr\left(\frac{\partial^2 u}{\partial x^2} + \frac{\partial^2 u}{\partial y^2} + \frac{\partial^2 u}{\partial z^2}\right) + Pr\,Ha^2\left(-u\sin^2\alpha + w\sin\alpha\cos\alpha\right) \tag{6}$$

$$\frac{\partial v}{\partial t} + u\frac{\partial v}{\partial x} + v\frac{\partial v}{\partial y} + w\frac{\partial v}{\partial z} = -\frac{\partial p}{\partial y} + Pr\left(\frac{\partial^2 v}{\partial x^2} + \frac{\partial^2 v}{\partial y^2} + \frac{\partial^2 v}{\partial z^2}\right) + Ra\,Pr\,\theta - Ha^2 v \tag{7}$$

$$\frac{\partial w}{\partial t} + u\frac{\partial w}{\partial x} + v\frac{\partial w}{\partial y} + w\frac{\partial w}{\partial z} = -\frac{\partial p}{\partial y} + Pr\left(\frac{\partial^2 w}{\partial x^2} + \frac{\partial^2 w}{\partial y^2} + \frac{\partial^2 w}{\partial z^2}\right) + Ra\,Pr\,\theta + Pr\,Ha^2\left(u\sin\alpha\cos\alpha - w\cos^2\alpha\right) \tag{8}$$

$$\frac{\partial \theta}{\partial t} + u\frac{\partial \theta}{\partial x} + v\frac{\partial \theta}{\partial y} + w\frac{\partial \theta}{\partial z} = \frac{\partial^2 \theta}{\partial x^2} + \frac{\partial^2 \theta}{\partial y^2} + \frac{\partial^2 \theta}{\partial z^2} \tag{9}$$

The boundary conditions, in the present study, are as follows:

$$\begin{cases} u = v = w = 0 \quad \text{on all walls} \\ \theta(x, y, 0) = +0.5; \qquad \theta(x, y, 1) = -0.5 \quad \text{at } 0 \le x, y \le 1 \\ \left.\dfrac{\partial \theta}{\partial x}\right|_{x=0} = \left.\dfrac{\partial \theta}{\partial x}\right|_{x=1} = 0 \quad \text{at } 0 \le y, z \le 1 \\ \left.\dfrac{\partial \theta}{\partial x}\right|_{y=0} = \left.\dfrac{\partial \theta}{\partial x}\right|_{y=1} = 0 \quad \text{at } 0 \le x, z \le 1 \end{cases} \tag{10}$$

Here x, y, and z are dimensionless coordinates varying along the horizontal and vertical directions, respectively; u, v, and w are the dimensionless velocity components in the x-, y-, and z-directions, respectively; θ is the dimensionless temperature, and p is the dimensionless pressure.

The following changes of variables are implemented in the equations above:

$$x = \frac{X}{L}, \qquad y = \frac{Y}{L}, \qquad z = \frac{Z}{L}, \qquad u = \frac{UL}{a}, \qquad v = \frac{VL}{a}, \qquad w = \frac{WL}{a}, \qquad \theta = \frac{T - T_0}{T_H - T_0}$$

$$p = \frac{PL^2}{\rho a^2}, \qquad Pr = \frac{\nu}{a}$$

$$Ra = \frac{g\beta\Delta T H^3}{a\nu}, \qquad Ha = BL\left(\frac{\sigma}{\mu}\right)^{1/2} \tag{11}$$

The reference temperature T_0 is chosen equal to $(T_H + T_C)/2$. B is the amplitude of the external magnetic field $\mathbf{B}$ controlled by the Hartmann number, which represents the ratio between Lorentz forces produced by the interaction of the current density J with the applied magnetic field and the viscosity forces.

Table 1
Grid independence tests for, $Ra = 10^5$, $Ha = 30$, and an inclination angle of the magnetic field about the horizontal direction $\alpha = 60°$.

Grid	*Nu*	(% Dev.)	U_{max}	(% Dev.)	W_{max}	(% Dev.)
32	1.9147	0.13	15.5747	−0.11	14.6956	1.76
48	1.9131	0.04	15.5888	−0.02	14.7384	−0.27
64	1.9125	0.01	15.5993	0.04	14.7344	−0.01
80	1.9122	–	15.5927	–	14.7361	–

Table 2
Comparison of the predicted Nusselt number *Nu* on the left or right walls of the cavity taken from Rudraiah et al. [6] and from Sathiyamoorthy and Chamkha et al. (HFF) [31] for the 2D case versus the present work.

Gr	*Ha*	*Nu* [Ref. 6] Case 2D	*Nu* [Ref. 31] Case 2D	*Nu* [PTW] Case 3D
2×10^4	0	2.5288	2.5439	2.3439
	10	2.2234	2.2385	2.0789
	10	1.0110	1.0066	1.0064
2×10^5	0	4.9198	5.0245	4.9116
	10	4.8053	4.9131	4.7164
	100	1.4317	1.4292	1.4171

3. Numerical method and validation

3.1. Method of solution

The governing nonlinear differential Eqs. (5)–(9), with the relevant boundary condition Eq. (10), have been solved numerically using the same methodology as that explained in details in previous works [27,28]. A staggered non-uniform mesh with second-order accurate finite volume method and the QUICK scheme have been used to minimize the numerical diffusion for the advective terms. Iterations are carried out until the normalized residuals of the mass, momentum and temperature equation become less than 10^{-8}, i.e. $\sum_{i,j} |\Phi_{i,j}^{it} - \Phi_{i,j}^{it-1}|^2 < 10^{-8}$. The generic variable Φ stands for u, v, w, p and θ; it indicates the iteration level; the subscript sequence (i, j, k) represents the space coordinates x, y, and z. Simulations were performed by using a finite volume home FORTRAN code named "NASIM" developed by the second author, which uses the numerical methodology described above.

3.2. Grid independency

Grid independence tests were performed using four grids involving 32, 48, 64, and 80 nodes in each direction (x, y, or z) of the cubic enclosure at $Ra = 10^5$, $Ha = 30$, and for the angle of inclination of 30° as shown in Table 1. The intermediate grid in each case was used since the solution obtained is very close to the solution for the finest grid (80^3) based on a comparison of the Nusselt numbers and u- and v-component velocity extrema (U_{max} and W_{max} in the mid plane $y = 0.5$). In order to ensure a compromise between the accuracy of the results and the CPU time, the numerical solutions presented in this study were acquired from a $48 \times 48 \times 48$ grid system. Such a grid presents very small differences compared to the finest one, and further increase in the number of grids produced essentially the same results as seen in Table 1.

3.3. Code validation

3.3.1. Critical Rayleigh number

The onset of Rayleigh–Bénard convection in an enclosure has also been investigated by several authors analytically, in terms of the linear stability theory, and numerically. For this purpose, we predicted numerically (with the help of the well-known mean-square method which will not be explained here for brevity) the Ra_c values corresponding to the onset of Rayleigh–Bénard convection when $Ha = 0$. According to the 2D-RB convection in a square cavity, our computed results reveal a value of 2585.82, which is in good agreement with the one obtained by Gelfgat [29] with a deviation of about 0.03%. On another hand, we obtain $Ra_c = 3325.87$ in the 3D RB convection, which is validated against the Ra_c value reported by Xiaowen Shan [30]. This result reveals a very good agreement.

3.3.2. 3D magnetoconvection tests

Furthermore, due to the luck of 3D-magnetoconvection benchmarks in the open literature, a second test has been also performed with an imposed magnetic field, and our results were compared to those of Rudraiah et al. [6] and to those of Sathiyamoorthy and Chamkha [31] in the 2D case. Computations have been carried out for various values of Ha (0–100 for a horizontally applied magnetic field, $\alpha = 0°$) and for two values of the Grashof number $Gr = 2 \times 10^4$ and 2×10^5 and $Pr = 0.054$ (liquid metals), as seen in Table 2. The results are close together, meaning that the 2D assumption remains valid. Generally, both 2D and 3D flows trend towards a large similarity, in particular for integral quantities.

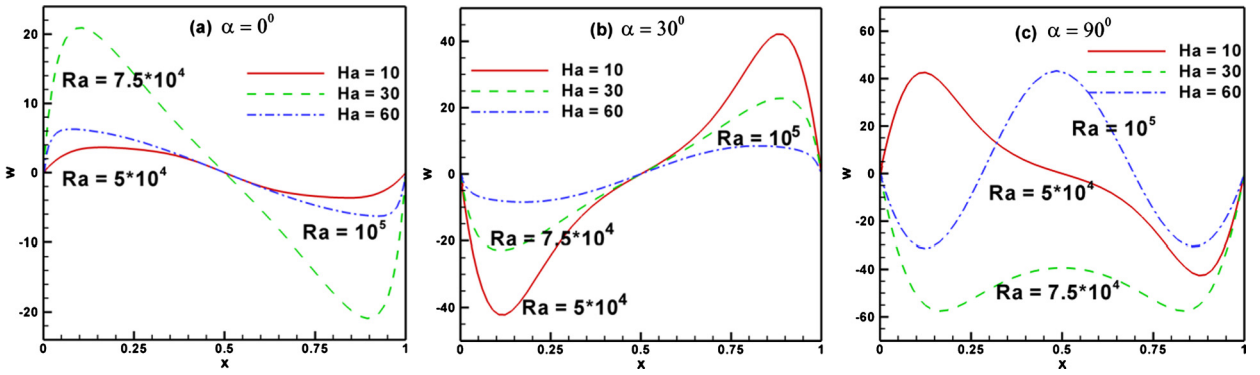

Fig. 2. (Colour online.) w-Velocity component profiles versus x-abscissa at the mid-plane ($y = 0.5$) for (a) $\alpha = 0°$, (b) $\alpha = 30°$, (c) $\alpha = 90°$, for different Rayleigh and Hartmann numbers.

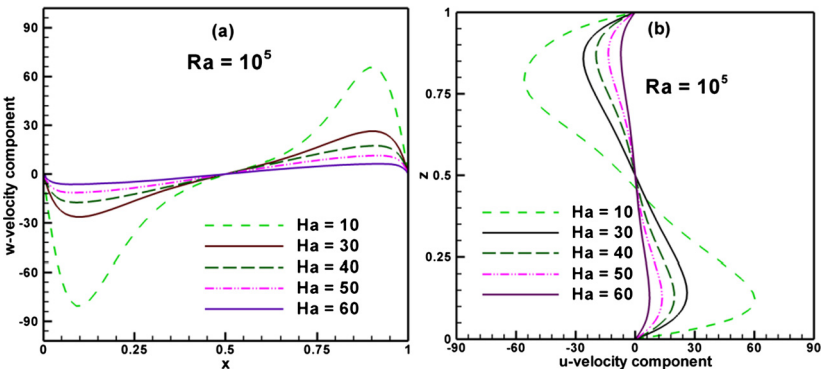

Fig. 3. (Colour online.) Velocity component profiles as a function of coordinates (a) $w(x)$, and (b) $u(z)$ at the mid-plane ($y = 0.5$) for $Ra = 10^5$ and an inclination angle $\alpha = 0°$.

4. Results and discussion

4.1. Choice of study parameters

In order to justify the choice of the selected parameters in the present study for convenience and brevity, we simply analyze the w-velocity component profiles in the vertical mid-plane $y = 0.5$. For this purpose, Fig. 2 exhibits the w-velocity component versus the x-abscissa for different Rayleigh and Hartmann numbers, and three different inclinations, namely 0°, 30°, and 90° about the horizontal plane at mid-plane $y = 0.5$. This figure shows the combined effects of the three governed parameters Ra, Ha, and the inclination angle α. Firstly, as seen from this figure, the magnitude of the velocity component in the z direction is enhanced in regions near the vertical walls, because there is a strong upward heat transfer transport. Usually, the convection becomes dominant by increasing Ra; this is not the case here (see Fig. 2a) as expected, because the imposed magnetic field tends to reduce significantly the buoyancy forces. In addition, as shown in Fig. 2b, the w-profile is inversed. Another configuration that demonstrates a different aspect of the flow when a vertical magnetic field is imposed ($\alpha = 90°$, Fig. 2c) is obtained for the same set of parameter (Ha, Ra). These observations deduced from Fig. 2 suggest that there is a kind of competition between the buoyancy effects represented by the Rayleigh number and the electromagnetic effects accounted for by the Hartmann number. For these reasons, an appropriate parameter choice is required, as conducted at the beginning of this study, to perform future numerical investigations.

4.2. RB magnetoconvection flow: case of a horizontal magnetic field

Typical components velocity profiles at the mid-plane ($y = 0.5$) in the case of an imposed horizontal magnetic field ($\alpha = 0°$) at fixed Rayleigh number ($Ra = 10^5$) and for different Hartmann values are shown in Fig. 3. Variations of both w- and u-velocity components versus x- and z-abscissa are drawn in Fig. 3a and Fig. 3b, respectively. We observe that for all the values of Ha considered in the range 10–60, by steps of 10, the magnitude of the velocity components decreases with increasing the magnetic field's intensity. As expected, with increasing the magnetic field, the strength of the recirculation flow vanishes. This is due to the fact that the magnetic forces become important when the intensity of the magnetic field is enhanced. Thus, the created Lorentz forces oppose progressively the buoyancy forces due to heating. On the other hand, w- and u-profiles reveal a perfect center symmetric trend for both x and z centerlines.

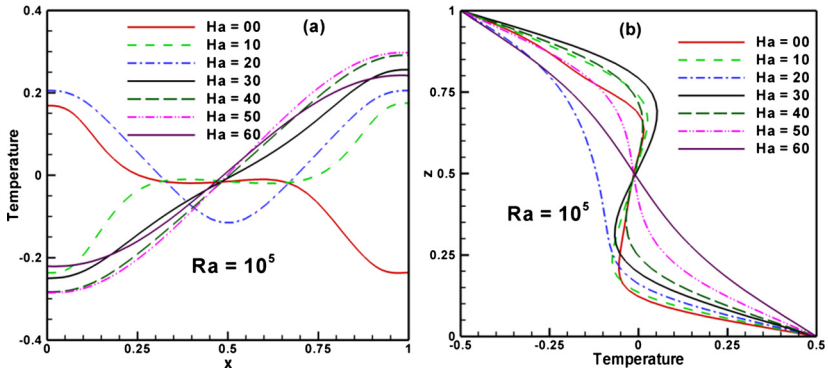

Fig. 4. (Colour online.) Temperature profiles at the mid-plane $y = 0.5$ versus (a) the x-abscissa at the centerline $z = 0.5$, and (b) the z-abscissa at the centerline $x = 0.5$ for different Hartmann numbers in the range from 0 to 60 for $Ra = 10^5$ and $\alpha = 0°$.

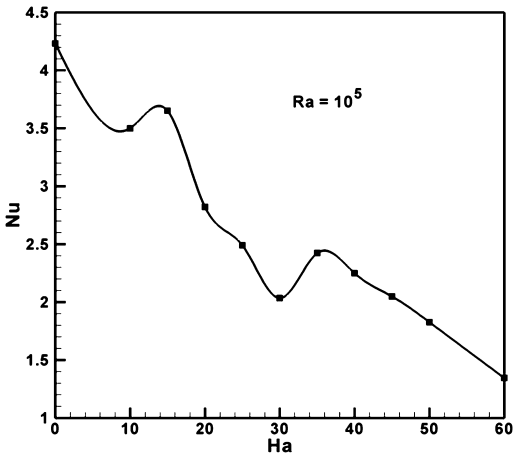

Fig. 5. Variation of the average Nusselt number versus the Hartmann numbers in the range from 0 to 60 for $Ra = 10^5$ and $\alpha = 0°$.

In Fig. 4, the temperature profiles along both the horizontal axis and the vertical axis are presented at the mid-plane $y = 0.5$ and for seven Hartmann number values. Similar temperature profiles are observed for higher-magnitude fields corresponding to $Ha = 30$, 40, 50, and 60, as shown in Fig. 4a. This subfigure shows that the left half of the axis is cold, while the right one is hot. This is because the right half axis is crossed by a hot ascending flow driven by the vertical component of the velocity vector (w) as mentioned earlier in Fig. 3. Negative dimensionless temperature values mean that the temperature therein is significantly lower than the reference temperature ($(T_C + T_H)/2$). However, a low magnetic field intensity ($Ha = 0$ and 20) shows a discernible effect on the temperature profile. In fact, the passage of $Ha = 0$ to 10 results in inverted profiles, while $Ha = 20$ reflects a different behavior, as expected. Furthermore, for lower values of Ha, the vertical centerline is heated along its lower half and on the contrary is cooled by its upper half. This is attributed to the enhanced role of convection in heat transport at the vicinity of the heated bottom wall. In addition, sudden variations in temperature profiles (Fig. 4b) in the vicinity of active horizontal walls explain important gradients in these places. Temperature profiles become linear when Ha increases sufficiently.

From this stage on, we can highlight the stabilization of the flow by increasing Ha. The influence of the Hartmann number on the average Nusselt number is presented in Fig. 5. This figure shows that the maximal heat transfer rate in the cavity diminishes up to $Ha = 10$, after which it increases, reaching a maximum value at Ha equal to 15, then decreases monotonously again up to $Ha = 30$. A new maximum is reached for $Ha = 35$, then the heat transfer rate decreases again, indicating a considerable reduction in the average Nusselt number at high Ha numbers. The occurrence of these two peaks may be due to the local occurrence of instabilities and bifurcation phenomena according to these values of the Hartmann number.

4.3. Magnetic field inclination effects

4.3.1. On flow patterns

In the following, we analyze the impact on the flow structure and heat transfer caused by a change in the direction of the magnetic field. For this purpose, w-velocity component profiles, as a function of the x-abscissa, have been depicted in Fig. 6 in the mid-plane $y = 0.5$ and for four different inclinations, namely, $\alpha = 0°$, 30°, 60°, and 90°. Three values of the

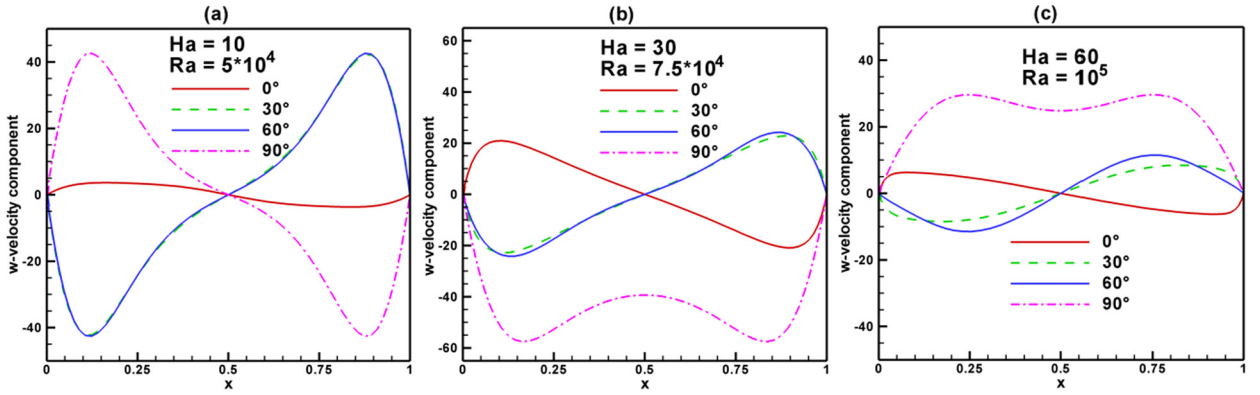

Fig. 6. (Colour online.) Velocity component profile $w(x)$ at the mid-plane ($y = 0.5$) for different inclination angles $\alpha = 0°$, 30°, 60° and 90° for various Hartmann numbers: (a) $Ha = 10$, (b) $Ha = 30$, and (c) $Ha = 60$.

Hartmann number ($Ha = 10$, 30, and 60) have been chosen and investigated. From Fig. 6, one can observe that regardless of the behaviour of these components, their magnitude decreases considerably by increasing the intensity of the magnetic field. First, if the Rayleigh–Bénard configuration is considered ($\alpha = 0°$), the heated particles localized at the bottom wall move to the left wall and migrate upward along the vertical wall. This motion is attributed to the positive w-component values, as seen in Fig. 6a. The colder particles are driven close to the ceiling and then downwards throughout the right vertical wall: the w-component takes negative values. Inclinations 30° and 60° show similar behaviors.

According to Eqs. (6) and (8), the components of the Lorentz force, in the vertical plane, are symmetric functions of $\sin\alpha$ and $\cos\alpha$ values of the two complementary angles 30° and 60°. Except for the lower values of Ha, there is either upward or downward movement of hot or cold particles under the only effect of the w-component, as can be seen in Fig. 6b and Fig. 6c.

Once more, we are interested in analysing the velocity isocontours by taking into account the combined effects of Ha, Ra, and of the tilt. Fig. 7 exhibits the u- and w-velocity isocontours for $Ha = 30$ and $Ra = 7.5 \times 10^4$ for different inclinations of the magnetic field in the mid-plane $y = 0.5$. As seen in Fig. 7, both u- and w-isocontours related to the RB configuration ($\alpha = 0°$) reveal different shapes compared to those for the rest of the inclinations. This is because the inertia of the flow has decreased markedly. For the rest of the inclinations ($\alpha = 30°$ and 90°), the flow stabilizes under the effect of Ha, which results in a rise of hot particles helped by the positive w-component followed by a downward movement of cold particles along the vertical walls using the u-velocity component. Hence, one can see two counter-rotating rollers revealing these movements in opposite directions.

With increasing the intensity of the magnetic field and the heating, as seen in Fig. 8, a major change in the flow's structure then appears at the differentially heated configuration ($\alpha = 90°$). In order to see the three-dimensional flow circulation within the enclosure (Fig. 8 shows some w-velocity component pathlines in the cubic enclosure for $Ra = 5 \times 10^4$, 10^5, two values of the Hartmann number, $Ha = 10$ and 60, and three different inclinations ($\alpha = 0°$, 30°, and 90°). As seen from this figure, the w-velocity component pathlines originating at the hot bottom wall (the point of origin is indicated by a filled circle at the hot wall: A (0.1, 0.1, 0.1)) passing through the fluid, and terminating at the cold wall (the point of termination is indicated by a filled circle at the cold wall: B (0.9, 0.9, 0.9)). The trajectories are colored in accordance to the vertical w-velocity magnitude. Hot walls always act as sources, while cold walls act as sinks for energy and motion. Generally, as can be seen from these subfigures, pathlines originate at the hot wall, pass through the fluid, and terminate at the cold wall; they are not necessarily closed curves. Due to RB instability encored at $\alpha = 0°$ and $Ha = 10$, Fig. 8a makes complicated spiral loops inside the fluid region, and finally terminates at the cold wall. When the intensity of the heating and magnetic field magnitude are kept unchanged, increasing the inclination of the magnetic field with respect to the horizontal ($\alpha = 30°$), the flow becomes symmetrical about the central vertical plane, so that the pathlines should be mirror images.

This becomes more marked if the differential heated cavity configuration is concerned ($\alpha = 90°$). As expected, increasing the magnetic field magnitude (Fig. 8d–f) provides strength stabilization and organization of pathlines. In addition, the w-velocity component of the fluid in the boundary layers near the two vertical walls is higher than the velocities along the cavity centre, as can be seen in Fig. 8d–e. This is because the hot fluid travels up the heated wall and then along the top ceiling toward the cold wall. A relatively colder fluid travels down the cold wall and then proceeds along the bottom heated wall toward the hot wall. According to the differentially heated cavity (90°), two distinct counter-clockwise circulating flows are generated, as seen in Fig. 8f.

To analyse the three-dimensionality nature of the flow, the isosurfaces of the transverse velocity component v for a specific value (-0.4) and a fixed inclination of 30° are shown in Fig. 9. From this figure, we can see an anti-symmetric structure about the mid-plane $y = 0.5$ for $Ha = 60$. This means that the three-dimensional effects are present and that the two-dimensional model can be a good approximation.

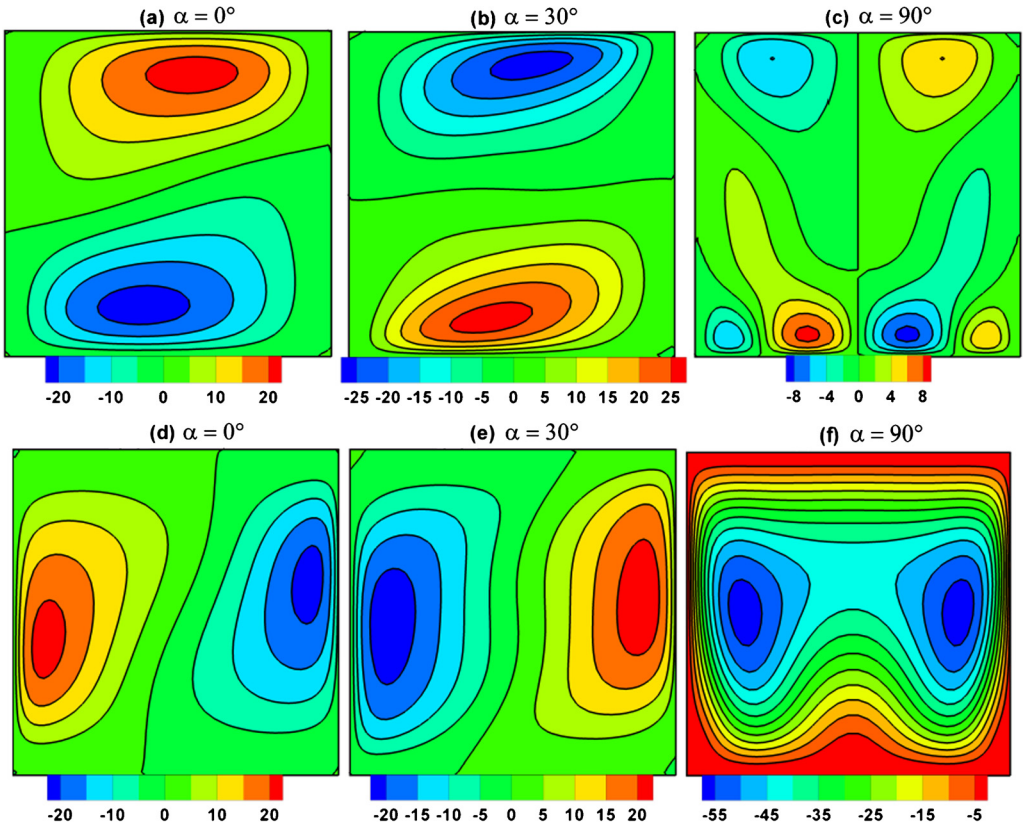

Fig. 7. (Colour online.) Velocity component isocontours at the vertical mid-plane $y = 0.5$ and different inclination angles $\alpha = 0°$, 30°, and $\alpha = 90°$ for $Ha = 30$ and $Ra = 7.5 \times 10^4$: (a)–(c) u-isocontours, and (d)–(f) w-isocontours.

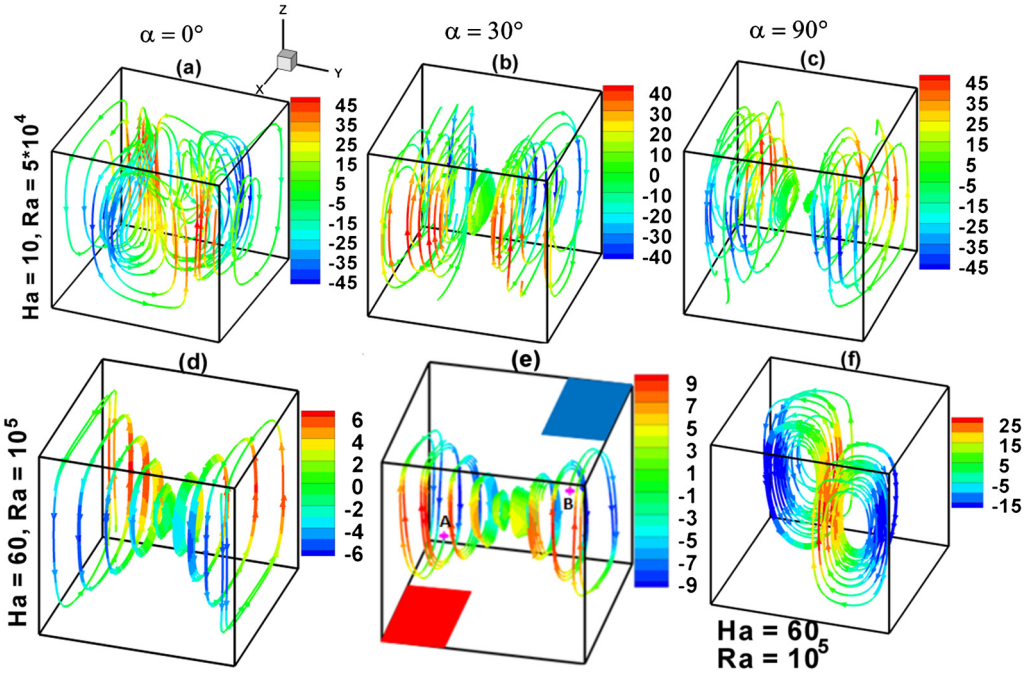

Fig. 8. (Colour online.) Fluid particle pathlines for different inclination angles $\alpha = 0°$, 30° and 90° for (a)–(c) $Ha = 10$ and $Ra = 5 \times 10^4$, and (d)–(f) $Ha = 60$ and $Ra = 10^5$.

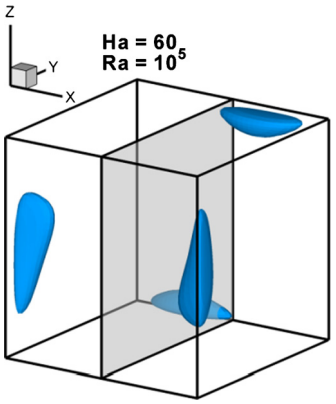

Fig. 9. (Colour online.) Isosurfaces of the transverse velocity component v for a specific value (-0.4) and a fixed inclination angle of 30°.

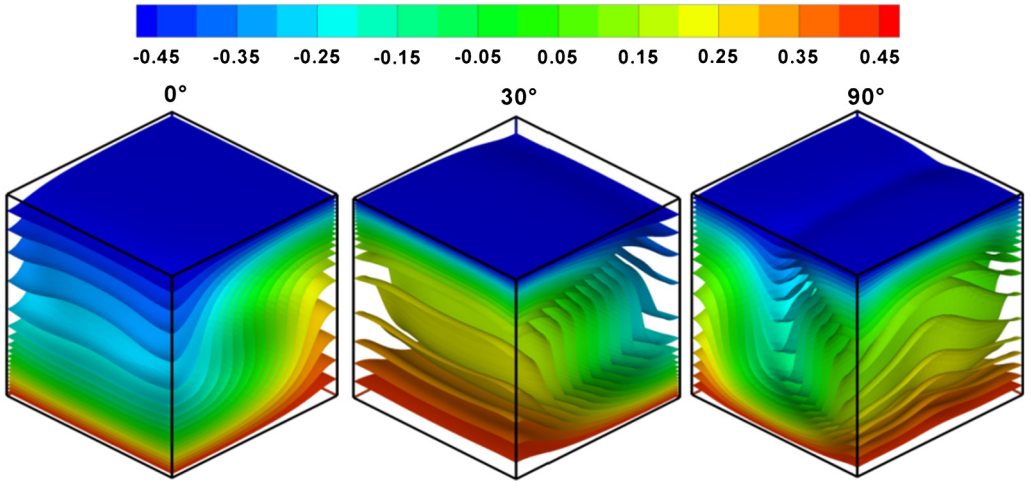

Fig. 10. (Colour online.) Temperature isosurfaces at the vertical mid-plane ($y = 0.5$) for three different inclination angles $\alpha = 0°$, 30° and 90° for Hartmann numbers $Ha = 30$ and 7.5×10^4.

4.3.2. On the temperature field

We are interested now in the temperature distribution of the central axis of the cavity, localized at mid-plane $y = 0.5$, under the effects of changes in the direction of the magnetic field. In fact, Fig. 10 shows three-dimensional isotherms in the cavity for $Ha = 30$, $\alpha = 0°$, 30°, 90°, and for a fixed Rayleigh number $Ra = 7.5 \times 10^4$. According to the Rayleigh–Bénard configuration ($\alpha = 0°$), the thermal gradient is high near the active sides due to three-dimensional instabilities. Once the magnetic field is inclined at 30°, one can observe a reversal flow illustrated by the fact that the heated and cooled parts are exchanged. When the magnetic field is applied in the vertical direction ($\alpha = 90°$), we can see a significant distortion of the temperature isosurfaces.

4.3.3. On heat transfer

The heat transfer rate across the fluid layer can be expressed in terms of average Nusselt number at the bottom wall ($z = 0$) as:

$$\overline{Nu} = -\frac{1}{AR}\int_0^1\int_0^1 \left.\frac{\partial\theta}{\partial z}\right|_{z=0} \mathrm{d}x\mathrm{d}y \tag{12}$$

In the following, we propose to quantify the heat transfer rate with the help of the average Nusselt number. For this purpose, Fig. 11 shows the variations of the average Nusselt number as a function of several parameters, namely Ha, Ra, and the inclination angle of the magnetic field about the horizontal direction. Fig. 11a illustrates the variation of the average Nusselt number versus all possible inclinations of the magnetic field. The optimal heat transfer rate appears when the magnetic field becomes vertical ($\alpha = 90°$). For this inclination, both buoyancy and magnetic forces act upward, corresponding to the aiding situation. A 33% rise in the average transfer rate was recorded (from Fig. 11a) between the two inclinations ($\alpha = 0°$ and 90°) for $Ha = 60$. Furthermore, as expected, the same figure exhibits a perfect symmetric profile of Nu by

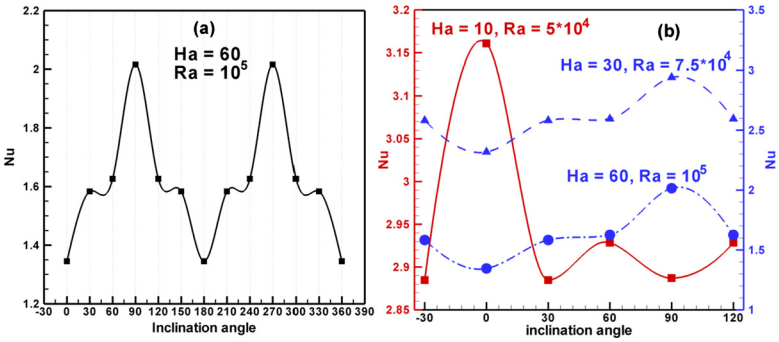

Fig. 11. (Colour online.) Variation of the average Nusselt number versus the inclination angle in the range from 0 to 120° for different Hartmann numbers.

scanning the magnetic field orientation from 0° up to 360°. This is due to the symmetry of the magnetic force components about the z vertical axis. In addition, this trend demonstrates the robustness of the numerical method to take into account the orientation of the magnetic field, which is the reason why the study has been restricted to orientations of the prime quadrant. For other pairs of values (Ha, Ra), as shown in Fig. 11b, there is a particular behaviour of the Nu profile at $Ha = 10$ and $Ra = 5 \times 10^4$. As mentioned earlier, according to these parameters, the flow undergoes a special regime characterized by instabilities and bifurcations. Only an increase of 8.6% has been estimated for this case. An analysis of Fig. 11b shows that with the increase of the intensity of the magnetic field Ha to 30, away from the bifurcation, Nu grows again to achieve about 21%. When an increase in the magnetic field is applied, for a fixed Ra number, a net reduction in heat transfer is imminent.

5. Conclusion

The effects of both the intensity and the orientation of the imposed magnetic field on the flow structure and the heat transfer rate within a cubical enclosure cavity heated from below have been investigated in the present study. Initially a suitable choice of study parameters has been performed to avoid complex situations due to instability and bifurcations.

The case of a horizontal field is first considered. Flow patterns have been analyzed in terms of typical components of the velocity profiles at the mid-plane ($y = 0.5$) for a fixed value of the Rayleigh number ($Ra = 10^5$) and different Hartmann values ranging from 0 to 30. Two contra-rotating rolls that are induced near the bottom and the ceiling in the opposite direction of the enclosure, except that corresponding to $Ha = 20$, which presents a strange behaviour, are observed. Temperature isosurfaces exhibit complex shapes due to the dominance of the convection effects in the absence of a magnetic field. The presence of a magnetic field is reflected by the distortion of the isosurfaces shapes not only in the center of cavity, but also at the vicinity of each side. The effect of the magnetic field is found to decrease the heat transfer rate considerably. In fact, the average Nusselt number profile presents two picks that may be due to the local occurrence of instabilities and bifurcation phenomena.

In second stage, the effect of the magnetic field inclination is concerned. It is obvious that this is related to the orientation of the magnetic force that can help or oppose the buoyant force. Given the symmetry property of the Lorentz force, the study has been restricted to orientations of the prime quadrant (0°–90°). For fixed values of Ha and Ra, the increasing inclination of the magnetic field with respect to the horizontal direction makes the flow undergoing a symmetrical shape about the central vertical plane, so the pathlines should be mirror images.

An optimal heat transfer rate appears when the magnetic field becomes vertical ($\alpha = 90°$). For this inclination, both buoyancy and magnetic forces act upward, corresponding to an aiding situation. A 33% rise in the average transfer rate was recorded between the two inclinations ($\alpha = 0°$ and 90°) for $Ha = 60$. A particular behaviour of the Nu profile at $Ha = 10$ and $Ra = 5 \times 10^4$ is observed. Only an increase of 8.6% has been estimated for this case. By increasing the magnetic field Ha to 30, away from the bifurcation, Nu grows again to achieve about 21%. When an increase in the magnetic field is applied, for a fixed Ra number, a net reduction in heat transfer is imminent.

References

[1] P.H. Kao, R.J. Yang, Simulating oscillatory flows in Rayleigh–Bénard convection using the lattice Boltzmann method, Int. J. Heat Mass Transf. 50 (2007) 3315–3328.
[2] M. Corcione, Effects of the thermal boundary conditions at the sidewalls upon natural convection in rectangular enclosures heated from below and cooled from above, Int. J. Therm. Sci. 42 (2003) 199–208.
[3] M. Cappelli, D. Orazio, C. Cianfrini, M. Corcione, Rayleigh–Bénard convection in tall rectangular enclosures, Int. J. Therm. Sci. 43 (2004) 135–144.
[4] S. Paul, P. Wahi, Mahendra K. Verma, Bifurcations and chaos in large-Prandtl number Rayleigh–Bénard convection, Int. J. Non-Linear Mech. 46 (2011) 772–781.
[5] N. Nithyadevi, P. Kandaswamy, S.M. Sundari, Magnetoconvection in a square cavity with partially active vertical walls: time periodic boundary condition, Int. J. Heat Mass Transf. 52 (2009) 1945–1953.
[6] N. Rudraiah, R.M. Barron, M. Venkatachalappa, C.K. Subbaraya, Effect of magnetic field on free convection in a rectangular enclosure, Int. J. Eng. Sci. 33 (1995) 1075–1084.

[7] A. Al-Mudhaf, A.J. Chamkha, Natural convection of liquid metals in an inclined enclosure in the presence of a magnetic field, Fluid Mech. Res. 31 (3) (2004) 221–243.
[8] H. Ozoe, Magnetic Convection, Imperial College Press, London, 2005.
[9] M. Pirmohammadi, M. Ghassemi, G.A. Sheikhzadeh, Effect of a magnetic field on buoyancy-driven convection in differentially heated square cavity, IEEE Trans. Magn. 45 (2009) 407–411.
[10] T. Bednarz, C. Lei, J.C. Patterson, H. Ozoe, Suppressing Rayleigh–Bénard convection in a cube using strong magnetic field — experimental heat transfer rate measurements and flow visualization, Int. Commun. Heat Mass Transf. 36 (2) (2009) 97–102.
[11] T. Tagawa, A. Ujihara, H. Ozoe, Numerical computation for Rayleigh–Bénard convection of water in a magnetic field, Int. J. Heat Mass Transf. 46 (2003) 4097–4104.
[12] S. Alchaar, P. Vasseur, E. Bilgen, The effect of a magnetic field on natural convection in a shallow cavity heated from below, Chem. Eng. Commun. 134 (1995) 195–209.
[13] T. Sophy, H. Sadatt, L. Gbahoue, Convection thermomagnétique dans une cavité différentiellement chauffée, Int. Commun. Heat Mass Transf. 32 (2005) 923–930.
[14] M.C. Ece, E. Büyük, The effect of an external magnetic field on natural convection in an inclined rectangular enclosure, J. Mech. Eng. Sci. 221 (2007) 1609–1622.
[15] M. Pirmohammadi, M. Ghassemi, Effect of magnetic field on convection heat transfer inside a tilted square enclosure, Int. Commun. Heat Mass Transf. 36 (2009) 776–780.
[16] D.C. Lo, High-resolution simulations of magneto-hydrodynamic free convection in an enclosure with a transverse magnetic field using a velocity–vorticity formulation, Int. Commun. Heat Mass Transf. 37 (2010) 514–523.
[17] H. Ozoe, K. Okada, The effect of the direction of the external magnetic field on the three-dimensional natural convection in a cubical enclosure, Int. J. Heat Mass Transf. 32 (10) (1989) 1939–1954.
[18] R. Mobner, U. Muller, A numerical investigation of three dimensional magnetoconvection in rectangular cavities, Int. J. Heat Mass Transf. 42 (1999) 1111–1121.
[19] I. Di Piazza, M. Ciofalo, MHD free convection in a liquid–metal filled cubic enclosure. – I. Differential heating, Int. J. Heat Mass Transf. 45 (7) (2002) 1477–1492.
[20] S. Kenjereš, K. Hanjalić, Numerical simulation of magnetic control of heat transfer in thermal convection, Int. J. Heat Fluid Flow 25 (2004) 559–568.
[21] B. Xu, B.Q. Li, D.E. Stock, An experimental study of thermally induced convection of molten gallium in magnetic fields, Int. J. Heat Mass Transf. 49 (2006) 2009–2019.
[22] T. Bednarz, E. Fornalik, H. Ozoe, Janusz S. Szmyd, John C. Patterson, L. Chengwang, Influence of a horizontal magnetic field on the natural convection of paramagnetic fluid in a cube heated and cooled from two vertical side walls, Int. J. Therm. Sci. 47 (2008) 668–679.
[23] D. Henry, A. Juel, H. Ben Hadid, S. Kaddeche, Directional effect of a magnetic field on oscillatory low-Prandtl-number convection, Phys. Fluids 20 (2008) 034104.
[24] H. Varshney, M. Faisal Baig, Rotating Rayleigh–Bénard convection under the influence of transverse magnetic field, Int. J. Heat Mass Transf. 51 (2008) 4095–4108.
[25] S. Sivasankaran, C.J. Ho, Effect of temperature dependent properties on MHD convection of water near its density maximum in a square cavity, Int. J. Therm. Sci. 47 (2008) 1184–1194.
[26] S. Bouabdallah, R. Bessaïh, Effect of magnetic field on 3D flow and heat transfer during solidification from a melt, Int. J. Heat Fluid Flow 37 (2012) 154–166.
[27] B. Ben-Beya, T. Lili, Transient natural convection in 3D tilted enclosure heated from two opposite sides, Int. Commun. Heat Mass Transf. 36 (2009) 604–613.
[28] B. Ben-Beya, T. Lili, Three-dimensional incompressible flow in a two-sided non-facing lid-driven cubical cavity, C. R. Mecanique 336 (2008) 863–872.
[29] A.Yu. Gelfgat, Different modes of Rayleigh–Bénard instability in two- and three-dimensional rectangular enclosures, J. Comput. Phys. 156 (1999) 300–324.
[30] Xiaowen Shan, Simulation of Rayleigh–Bénard convection using a lattice Boltzmann method, Phys. Rev. 55 (3) (1997) 2780.
[31] M. Sathiyamoorthy, A.J. Chamkha, Natural convection flow under magnetic field in a square cavity for uniformly (or) linearly heated adjacent walls, Int. J. Numer. Methods Heat Fluid Flow 22 (2012) 677–698.